PROCEEDINGS OF THE ROYAL SOCIETY A MATHEMATICAL, PHYSICAL & ENGINEERING SCIENCES

Droplet Combustion near a Cold Surface

S. Chandra and C. T. Avedisian

Proc. R. Soc. Lond. A 1990 **429**, doi: 10.1098/rspa.1990.0070, published 8 June 1990

Proc. R. Soc. Lond. A **429**, 481–503 (1990)
Printed in Great Britain

Droplet combustion near a cold surface

By S. Chandra and C. T. Avedisian
Sibley School of Mechanical and Aerospace Engineering, Cornell University, Ithaca, New York 14853-7501, *U.S.A.*

(*Communicated by D. B. Spalding, F.R.S. – Received* 22 *August* 1989)

[Plates 1–5]

The combustion of a liquid droplet adjacent to a cold surface was studied experimentally. To isolate the effect of the proximity of the droplet to the surface, the ambient pressure (0.101 MPa), liquid composition (*n*-heptane), initial liquid volume (7×10^{-4} ml), surface material (quartz) and ambient temperature (20 ± 2 °C) were held constant. A range of distances L from the surface were studied ($1\text{ mm} < L < \infty$). Both horizontal and vertical surface orientations were examined. A more limited set of experiments were carried out in a low gravity (i.e. low buoyancy) environment to provide a basis of comparison with relevant theoretical analyses.

The flame shape, soot formation, fuel condensation, and droplet burning rate were all found to be strongly affected by the proximity of the droplet to the surface. For sufficiently large L the flame was observed to be closed around the droplet throughout burning. As L decreased, the flame was truncated. The droplet burning rate decreased as the droplet was brought progressively closer to the surface (in qualitative agreement with a relevant closed form potential flow solution to the analogous problem of a droplet burning adjacent to an adiabatic surface) and the burning rate of a droplet adjacent to a vertical surface was larger than for a horizontal surface. Surface orientation effects were observed to be absent for burning at low gravity. The extent of sooting as revealed by the flame colour was decreased, and fuel vapours condensed in a lens-like shape on the surface, as L was sufficiently reduced.

Nomenclature

B	transfer number	f	stoichiometric fuel–air mass ratio
C_1, C_2	constants	$[F]$	fuel concentration around droplet
c_{pv}	heat capacity of vapour	$[\mathring{F}]$	fuel reaction rate
d	diameter of quartz fibre	g	acceleration due to gravity
D	equivalent diameter of droplet defined in equation (1)	g_0	acceleration due to Earth normal gravity
D_o	initial equivalent diameter	H_F	flame height above the droplet centre
D_v	longitudinal diameter of droplet	H_L	distance to the start of the
D_h	lateral diameter of droplet		
Da	Damköhler number		

	yellow luminous zone from the droplet centre
k_v	vapour thermal conductivity
K	combustion rate
K_∞	combustion rate of a droplet as $L \to \infty$
K_v	combustion rate of a droplet near a vertical surface
K_h	combustion rate of a droplet above a horizontal surface
L	distance from the fibre tip to the quartz surface
L_0	initial droplet to surface distance
$\mathring{m}$	mass evaporation flux from droplet surface
$[O_2]$	oxygen concentration
q_s	heat flux into the surface
R	gas constant
t	time from droplet ignition
t_r	characteristic time for fuel to travel from drop to the quartz surface
t_c	characteristic time for fuel combustion
T_f	characteristic flame temperature
T_s	temperature of quartz surface
ΔT_s	change in surface temperature
v_a	velocity with which drop approaches surface
v_s	characteristic velocity with which fuel vapour leaves the drop
Y_O	mass fraction of oxygen
$Y_{O,\infty}$	ambient oxygen mass fraction
Y_f	mass fraction of fuel
δ	minimum distance between drop and surface
ϵ	thickness of vapour layer between the flame and the surface
ξ^*	function of L/D, defined in equation (3)
ξ_f	bispherical coordinate of flame surface
η_f	bispherical coordinate of flame surface
θ	angle measured from the bottom of the drop
ρ_l	density of liquid
ρ_v	density of vapour
λ	function defined in equation (4*c*)

1. Introduction

The evaporation and burning characteristics of a droplet which is near a hot solid surface are different than for a droplet in an unbounded ambience (Tamura & Tanasawa 1959; Gottfried *et al.* 1966; Karasawa *et al.* 1986; Chandra & Avedisian 1988). The flame shape, burning rate, and extent of sooting in particular are influenced by the proximity of the droplet to the surface. The combustion of a droplet near a cold surface introduces the additional prospect of fuel vapour condensation on the surface during combustion and of a more pronounced influence of the surface on the amount of soot formed because of increased heat transfer from the flame to the surface and a concomitant reduction of flame temperature. An initially cold surface is also more susceptible to thermal stresses due to sudden contact with the hot combustion gases surrounding the burning droplet.

This work was undertaken to study experimentally the burning of a single isolated fuel droplet near a cold surface. The aspects of droplet burning of interest were (1) droplet burning rate, (2) flame shape around the droplet, (3) flame

temperature, (4) flame colour (as a measure of soot formation), (5) evolution of solid surface temperature, and (6) condensation of fuel vapour on the solid surface. While a droplet moving toward and impacting on a surface is undoubtedly of practical interest as it relates to industrial furnaces and spray-fired incineration of hazardous wastes, and direct injection engines, it is difficult to make controlled measurements for moving droplets that isolate the effect of the proximity of the droplet to the surface. The present approach was therefore to essentially 'freeze' the droplet's position by constraining it with a support fibre at a specified distance from the test surface for the duration of its burning history and then to record the droplet burning characteristics for that position. In this respect the present results may be relevant to a kind of quasi-steady limit of burning (i.e. the ambient conditions being considered to adjust instantaneously to changes in both droplet size and position from the surface), and to droplets that are moving with a stokesian velocity toward the surface.

The experimental method consisted of positioning the test droplet at a known distance from the solid surface, igniting the droplet by an electric spark, and then recording its burning history by photographic means. The principal parameter was the distance of the droplet from the wall. The fuel (*n*-heptane, C_7H_{16}), initial droplet volume (7.0×10^{-4} ml), ambient temperature (20 ± 2 °C), and ambient pressure (0.101 MPa) were held constant. Both horizontal and vertical surface orientations were examined. The surface was initially at the ambient temperature. The bulk of the experiments were carried out at Earth normal gravity, though additional data were obtained in a low gravity environment. These latter observations were made to provide a basis of comparison with relevant theoretical analyses which have neglected buoyancy effects.

2. Apparatus

Figure 1 shows a schematic diagram of the experimental apparatus. The main components were: a quartz fibre mounted on a support arm from which the droplet was suspended; a hypodermic needle used to form the droplet; spark electrodes to ignite the drop; a quartz surface near which the droplet was held; and a video–photographic system to record the combustion history of the droplet.

A droplet was formed at the tip of a 0.15 mm diameter stainless steel hypodermic needle by forcing fuel through it from a Sage Instruments model 341A syringe pump at a flow rate of 0.69 ml min^{-1}. The droplet was then transferred to a 0.05 mm diameter quartz fibre by essentially touching the point of the needle to the fibre tip. The tip of the fibre was fashioned into a 0.15–0.20 mm spherical bead (the bead size was greater than that of the hypodermic needle to allow transfer of the droplet). Droplets with equivalent diameters of 1.1 ± 0.05 mm could be formed (corresponding to a volume of 7.0×10^{-4} ml) with this method.

The fibre support was attached to a traverse that allowed positioning of the fibre tip near the test surface to within ± 0.002 mm. The distance from the centre of a suspended droplet to a vertical surface remains constant as the droplet becomes smaller during combustion. However, the distance from the centre of a droplet

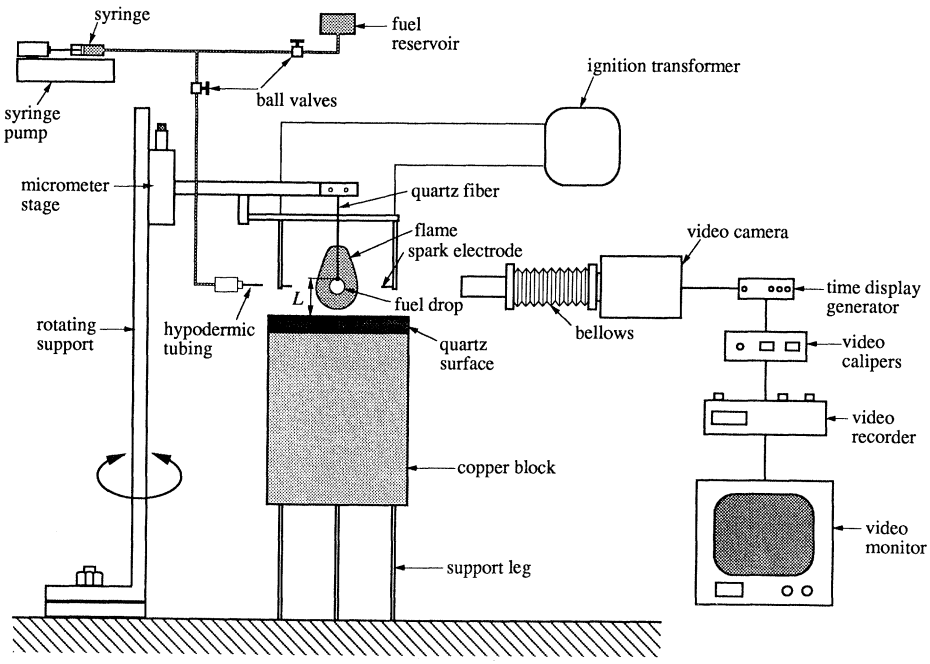

FIGURE 1. Schematic diagram of apparatus.

suspended above a horizontal surface changes as the droplet size diminishes. To avoid any ambiguity in defining the droplet to surface distance, the distance (L) from the tip of the suspension fibre to the surface was used as a length scale.

The droplet was held near the centre of a flat quartz disk, 76.2 mm in diameter and 3.2 mm thick. Quartz was selected so as to minimize heat losses from the flame, thereby approximating an adiabatic wall. The reason for simulating this boundary condition is discussed in §3.1.

The droplet was ignited by means of a 20 ms duration electric spark across two electrodes straddling the drop. The droplet was centrally placed between the two electrodes. The electrodes were made from 0.5 mm diameter stainless steel needles which were tapered to a fine point. The electrode tips were placed 10 mm apart to avoid interfering with the flame surrounding the droplet.

The droplet diameter was measured using a Video Logic CDR 460 video camera to which was attached a Nikon 105 mm lens and extension bellows. Front lighting was furnished by a General Radio 1538A strobe that was driven by the camera. The strobe provided 1 μs duration images at a rate of 30 s^{-1}, thus eliminating any blurring of the image. A time display with a resolution of 0.1 s was added to the video image by a Vicon V240TW timer.

Figure 2 shows representative video images, viewed on an Audiotronics 330 mm black and white monitor, of a burning heptane droplet at two different times during the combustion period. Due to the intense light of the strobe, the flame surrounding the drop cannot be seen. Diameter measurements were made directly from the monitor using a Model 306 Colorado Video Caliper. The caliper

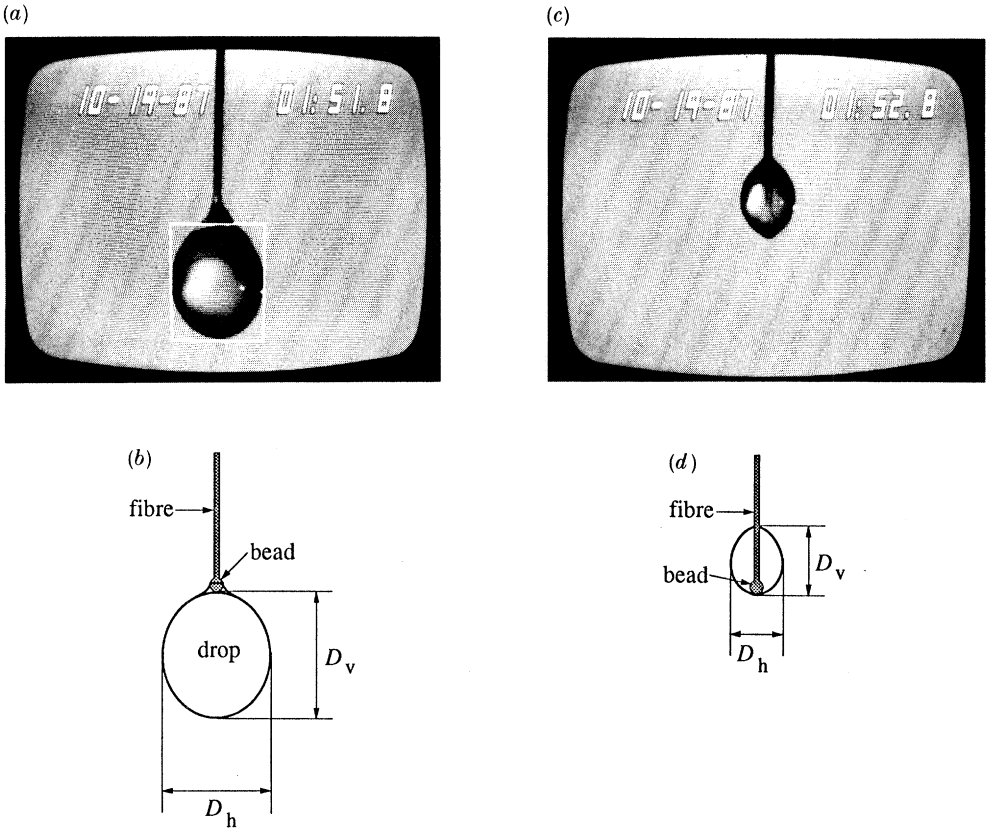

FIGURE 2. (*a*) Video image of suspended droplet under normal gravity at the start of burning. The white rectangle is the video caliper box. (*b*) Definition of lateral and longitudinal diameters at the start of burning. (*c*) Video image showing droplet drawn up the fibre towards the end of burning. (*d*) Diameter definition towards the end of burning.

electronically superimposed on the image a rectangle of variable size (shown in figure 2*a*) and allowed linear dimensions of the vertical (D_v) and horizontal (D_h) diameter to be measured to within an accuracy of 0.01 mm. The dimensions of the 'box' shown in figure 2*a* were calibrated with the aid of a spherical ball bearing of known diameter. The image of the drop shown in figure 2 appears slightly elongated longitudinally due to distortions caused by the curvature of the video monitor. This distortion was compensated for by separately calibrating measurements in the vertical and horizontally directions. The accuracy of this data extraction method was independently compared with a computer-based system (Anderson 1989) and found to agree within 10%. This difference appeared to be due to uncertainties in identifying the boundary between the droplet and ambience on the photographic image.

The test droplet was initially suspended from the bead at the tip of the fibre, its weight being supported by surface tension forces acting on the fibre, in the manner depicted in figure 2*a*. The droplet was not spherical because of the distortion caused by the fibre and the effect of gravity. The non-spherical shape of the

droplet necessitated defining an equivalent droplet diameter. We based this equivalent diameter on measurements of the horizontal and vertical dimensions of the droplet, D_v and D_h shown in figure 2.

The determination of D_v was somewhat dependent upon whether the experiments were carried out at Earth normal gravity or at low gravity. At normal gravity the initial droplet has the shape shown in figure 2*a*. Some small amount of liquid is drawn around the bead and up the fibre where it resides with a shape defined by the geometry of the bead and the contact angle of the liquid which is commensurate with the temperature. D_v was defined as shown in figure 2*b*, starting at the highest location on the droplet surface and neglecting the liquid drawn up around the bead. As the droplet burned and its mass correspondingly reduced, surface tension ultimately drew the droplet up the fibre to the shape shown in figure 2*c*. This occurred after about 70% of the droplet lifetime after which time no further data were taken. The small droplet volume, coupled with the severe distortion of the droplet shape, made it difficult to define a meaningful droplet shape and burning rate which was not effected by the fibre.

At low gravity, the droplet immediately assumed the shape shown in figure 2*c* as gravity was effectively removed so that surface tension forces caused the droplet to climb up the fibre. Data were taken with this droplet shape for the duration of the period of low gravity, which spanned between 40% and 60% of the droplet lifetime. The effective droplet size after this time was still large enough that fibre effects on heat transfer to the droplet were negligible.

Several definitions of an equivalent diameter of a fibre supported droplet can be envisioned: the diameter of a sphere of volume equal to the drop; the diameter of a sphere of equal surface area; the diameter measured at 45° to the horizontal (Kumagai *et al.* 1971); or simply the lateral or longitudinal dimension (D_v or D_h). All definitions except the naive choice of D_h or D_v yielded equivalent diameters that differed by at most 3%. Based on the shapes shown in figure 2*b* and *d* an equivalent droplet diameter was defined to correspond to a sphere with a volume that was equal to a volume of an ellipse rotated about its vertical axis:

$$D = (D_h^2 D_v)^{\frac{1}{3}}. \tag{1}$$

An influence of the quartz fibre on the droplet burning history could arise because of its effect on the heat conducted from the flame to the droplet through the fibre. A simple calculation assuming one dimensional heat conduction through the fibre, though, shows that the heat conducted through a 50 μm diameter quartz fibre is less than 2% of the total heat input to the droplet from the combustion reaction for the period of observation (Chandra 1990). As the fibre diameter is increased the fibre exerts a larger influence on the burning history. For example, a 200 μm fibre would increase heat transfer to the droplet by 10%. It is recognized that the fibre support method may not be useful for fuels that experience microexplosions during their combustion or extinction late in the droplet burning history.

Photographs of the flame surrounding the droplet were taken using a Nikon F3 camera equipped with a 105 mm *f*4 macrolens and bellows. The bellows were extended 110 mm and the front of the lens was placed at a distance of 140 mm

from the droplet. Under normal gravity conditions colour photographs were taken of the flame using Fujicolor 1600 ASA film. Figure 5 shows examples of photographs, taken at a rate of 3 frames per second, of the entire burning history of a drop. The camera lens was opened to an aperture of $f4$. Camera shutter speeds varied from 1/60 s when the droplet was far from the surface and the flame was brightly luminous, to 1/15 s for a drop close to the surface when the flame became blue and its luminosity decreased. All ambient light was extinguished while the photographs were taken to permit the flame to be seen clearly.

Photographs were also taken of the fuel and water vapour condensing on the quartz surface by using the above described camera set-up but now with Kodak TMAX 400 ASA film. The surface was illuminated from the front by using two GE FHX 13 V bulbs aligned with their centres level with the surface such that their light was shining parallel to it. This lighting made the transparent water vapour film on the surface appear dark and therefore easier to photograph. The camera was angled above the horizontal surface at approximately 30° to provide somewhat of a three-dimensional perspective. The flame was not visible in these photographs because of the light intensity used.

Gas temperatures surrounding the burning droplet were measured using a 25 μm diameter platinum–10 % rhodium thermocouple with a 50 μm diameter bead. The bead was coated with a mixture of beryllium oxide and yttrium oxide (Kent 1970) to prevent any catalytic reactions on the thermocouple surface. Temperatures were measured only in the blue, non-luminous region of the flame, to prevent soot accumulation on the thermocouple bead. The thermocouple was mounted on a vernier stage that allowed the bead to be moved both horizontally

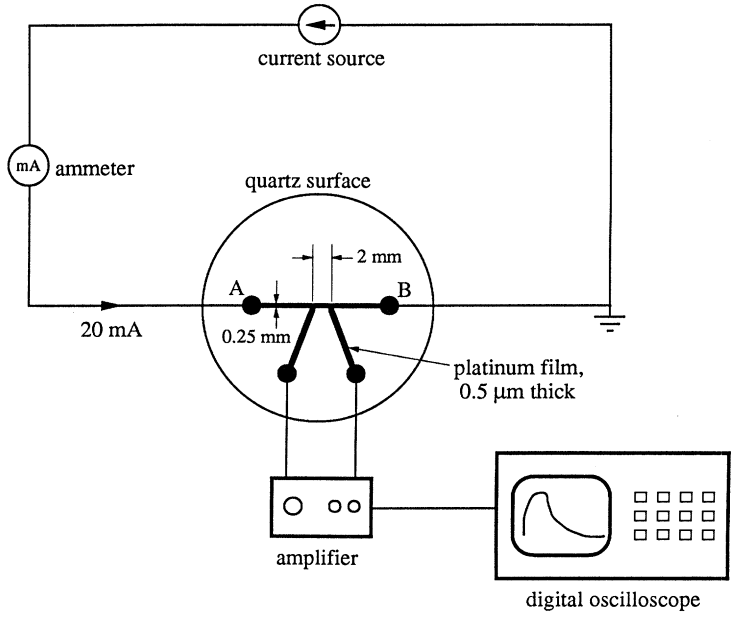

FIGURE 3. Schematic diagram of apparatus for surface temperature measurement using a platinum thin film sensor.

and vertically relative to the drop with an accuracy of 0.1 mm. During the burning of the droplet the signal from the thermocouple was amplified by using an Omega Omni Amp II B amplifier and recorded on a HP 54100D digital oscilloscope. The temperatures measured were corrected for radiation losses (Kaskan 1957) from the thermocouple. Corrections of up to 175 K were required at the highest uncorrected temperatures.

Surface temperature changes of the quartz surface were also measured during combustion. A platinum thin film sensor was fabricated by sputtering platinum on the quartz surface through a mask machined from 0.25 mm thick stainless steel in the shape shown in figure 3. The platinum film was 0.25 mm wide and 0.5 μm thick, with a resistance over the length A-B of approximately 100 Ω. Through this length was passed a constant 20 mA current. The droplet was suspended directly over the centre of the platinum film and ignited. The change in the voltage drop across the centre 2 mm of the platinum film was amplified and recorded on the digital oscilloscope (Chandra 1990). The voltage drop was converted to temperature by comparison with a calibration curve that was obtained by placing the quartz surface in an oven at a known temperature and recording the voltage drop across the sensor as a function of the surface temperature. The inferred temperatures were accurate to within ± 1 °C.

3. Results and discussion

3.1. *Comparison of theory with experiment*

The problem of a single droplet burning near a solid surface has not been solved. A related problem has been studied which involves two burning droplets of equal diameter in which the centre-to-centre distance between the droplets is constant throughout the burning history (Umemura *et al.* 1981), a so-called tandem droplet problem. This tandem droplet solution can be applied to the case of a single drop burning near a surface because a plane of symmetry exists between the two drops which is equivalent to an adiabatic surface. Formulations which emerge from the analysis that are amenable to experimental verification are predictions of the flame shape and the droplet burning rate. It is acknowledged, though, that quantitative comparisons may *a priori* be expected to fail because the experimental conditions do not conform in all respects to the assumptions upon which the model is based (e.g. that of assuming a single step chemical reaction at the flame front; the neglect of buoyancy, soot formation, and heat transfer to the solid surface; assuming constant properties, etc.). Nevertheless, the idealized solution to the tandem droplet problem can provide a useful start for understanding the mechanisms which control the burning of a droplet near a wall.

The shape of a flame surrounding a burning droplet which is constrained at a distance L from the surface is defined by the location where $Y_f = Y_O = 0$. On this basis an equation for the flame shape is given by the following expression (Umemura *et al.* 1981):

$$\sqrt{[2(\cosh \xi_f - \cos \eta_f)]} \sum_{n=0}^{\infty} [1 - \tanh (n+\tfrac{1}{2})\,\xi^*]\, P_n(\cos \eta_f) \cosh (n+\tfrac{1}{2})\,\xi_f = \frac{\ln (1+Y_{O,\infty} f)}{\ln (1+B)}, \quad (2)$$

where η_f and ξ_f are the coordinates of the flame surface in the bispherical system, P_n is the Legendre polynomial of order n and B is the so-called transfer number (Williams 1985). ξ^* is defined by

$$\xi^* = \operatorname{arccosh}(2L/D), \tag{3}$$

where L is the distance of the droplet from the surface and D is the droplet diameter. The right-hand side of (2) is a function of fuel properties and the ambient conditions so that the flame shape depends only on the ratio L/D. Equation (2) is based on a single step chemical reaction that produces CO_2 and H_2O so that in principle the flame would not be visible. In reality the presence and oxidation of other carbon containing compounds and radicals in the combustion products produce a blue colour that is used here to define the flame boundary.

The combustion rate, $K\,(\equiv -\mathrm{d}D^2/\mathrm{d}t)$, may be expressed as

$$K = \lambda K_\infty, \tag{4a}$$

where K_∞ is the burning rate for a droplet in an unbounded ambience (Williams 1985),

$$K_\infty = 8(k_v/\rho_1 c_{pv}) \ln(1+B), \tag{4b}$$

and

$$\lambda = \sinh \xi^* \sum_{n=0}^{\infty} [1 - \tanh(n+\tfrac{1}{2})\xi^*]. \tag{4c}$$

λ expresses the influence of the surface and depends only on L/D.

Figure 4 shows predicted flame shapes obtained by using appropriately estimated properties of n-heptane (Vargaftik 1975) and the far field ambience ($Y_{O,\infty} = 0.23$). At small L/D the flame does not close around the droplet surface. At large L/D the flame completely surrounds the droplet and its shape is nearly spherical for sufficiently large L/D because buoyancy and axial vapour flows around the droplet have been neglected in deriving (2). The transition between these two régimes (figure 4*b*) is predicted to occur at $(L/D)_{crit} \approx 35$ for heptane.

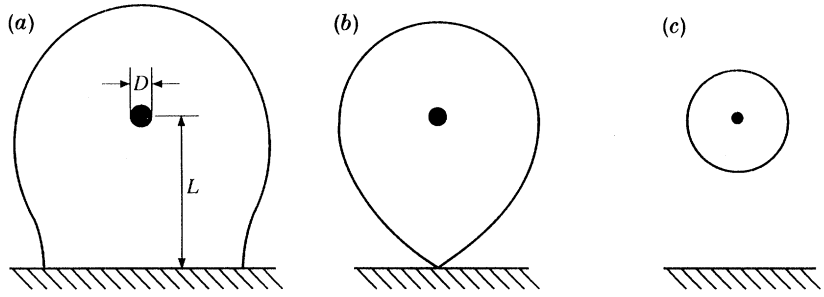

FIGURE 4. Calculated flame shapes for three different values of L/D: (*a*) $L/D = 29$, (*b*) $L/D = 35$, (*c*) $L/D = 61$.

Figure 5, plates 1 and 2, shows a series of colour photographs (to facilitate identification of the flame boundary) of an n-heptane droplet burning at Earth normal gravity near a horizontal (figure 5*a*) and vertical (figure 5*b*) surface. A photograph is identified by the coordinate $[L, t]$. Each row (where L is constant and D decreases) records the burning history of a single droplet. Along each

column L is increasing while D is approximately constant. The photographs were taken at intervals of $\frac{1}{3}$ s. The surface is illuminated by the ignition spark in the first photograph in each row and the suspension fibre can be seen extending vertically above the drop.

At large L/D the flame closes around the drop (cf. figure 4*c* and [3, $\frac{5}{3}$] in figure 5*a*), whereas as L/D decreases the flame opens as shown in figure 5*a* (e.g. [3, $\frac{1}{3}$]). The transition from an open to a closed flame occurs at $L/D \rightarrow (L/D)_{\text{crit}} \approx 4$ (e.g. [3, 1] and [3, $\frac{4}{3}$] in figure 5*a*) for burning near both the horizontal and vertical surface. The shape of the flame is different for the two surface orientations even though the flame closes around the droplet at about the same value of L/D.

The measured $(L/D)_{\text{crit}}$ is about an order of magnitude smaller than prediction. A sensitivity analysis of physical property estimates in (2) failed to account for this large difference. Other possible reasons for this difference may be that (*a*) natural convection is present in the experiments, (*b*) the surface is not adiabatic, and (*c*) soot formation as revealed by the yellow colour that is characteristic of radiation of soot particles (cf. the wake region of the droplets shown in figure 5) is not accounted for in the theory.

To assess the influence of buoyancy-induced gas flows around the droplet, observations were made in a low gravity (i.e. low buoyancy) environment using a drop tower facility (Avedisian *et al.* 1988) to minimize buoyancy effects. The apparatus shown in figure 1 was placed within an instrumentation package and then released into free fall. The droplet was ignited 200 ms after release. Grashof numbers based on the droplet diameter burning in the moving frame of reference were on the order of 10^{-3}, in contrast to the value of 10^{-1} which characterized the experiments carried out at $g/g_0 = 1$. A single 35 mm photograph of the flame was taken 330 ms after ignition using Kodak TMAX ASA 3200 black and white film which was push processed at 25000 ASA. The film was developed for 18 min in TMAX developer at 21 °C.

Figure 6, plates 3 and 4, shows representative photographs of *n*-heptane droplets. For each value of L, two photographs of the flame are shown: one taken at low gravity ($g/g_0 \approx 10^{-3}$ and generically labelled $0g$), and the other taken at normal gravity conditions ($g/g_0 = 1$ or $1g$), the latter of which are essentially the same as shown in figure 5. The position of the quartz surface is indicated by the white line.

As shown in figure 4 the 'flame' closes around the droplet when $(L/D) \geqslant 8$ for both the 'horizontal' (figure 6*a*) and 'vertical' (figure 6*b*) surface, which is closer to the prediction but is still much smaller than it. This persistent discrepancy with theory calls into question the role of what is conjectured to be soot on $(L/D)_{\text{crit}}$ through its possible effect on obscuring the identification of the flame boundary and its effect on the location of the reaction zone.

The luminosity of the soot could create some ambiguity in the identification of the flame boundary. The yellow regions of the flame shown in the colour photographs of figure 5 appear white when black and white film is used (figure 6). At $L = 2$ mm in figure 6, a faint luminous soot zone is visible above the drop which is suggestive of the reaction zone residing outside the soot boundary. The identification of such a zone is more difficult as L increases because of the

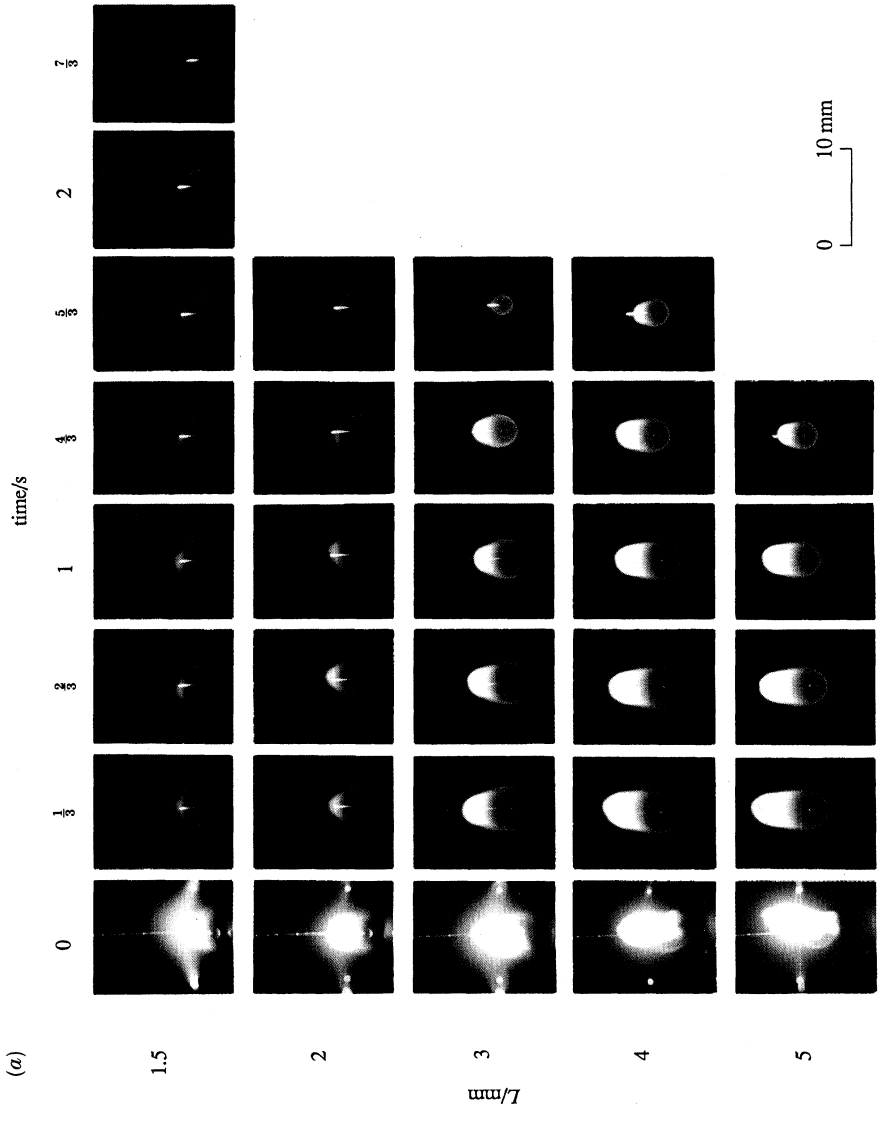

FIGURE 5*a*. Combustion of a droplet suspended over a horizontal surface at normal gravity.

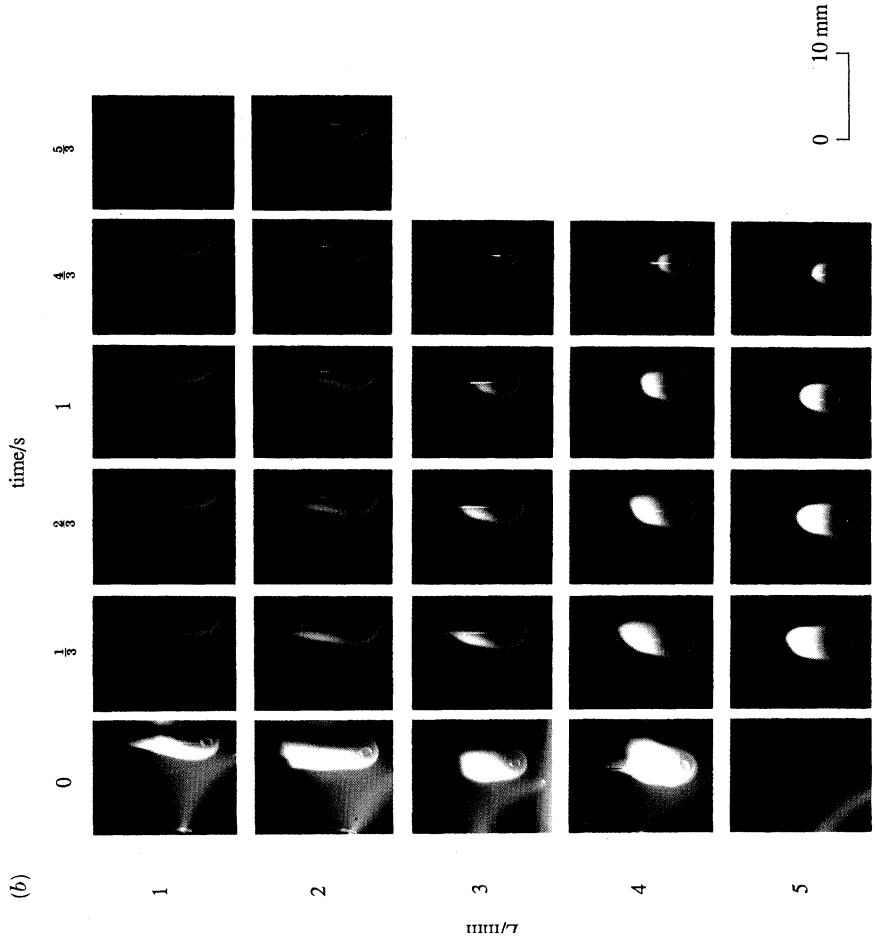

FIGURE 5*b*. Combustion of a droplet suspended near a vertical surface at normal gravity.

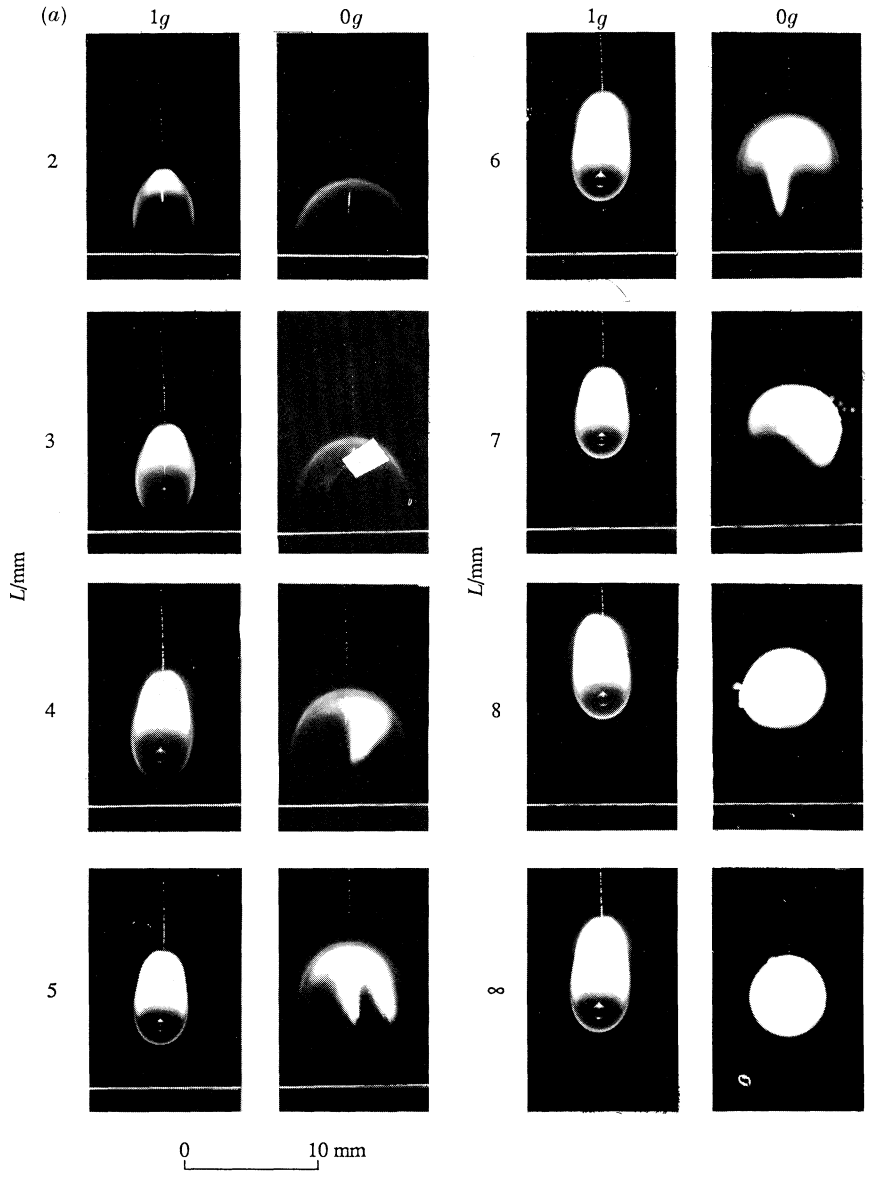

FIGURE 6(*a*). For description see opposite.

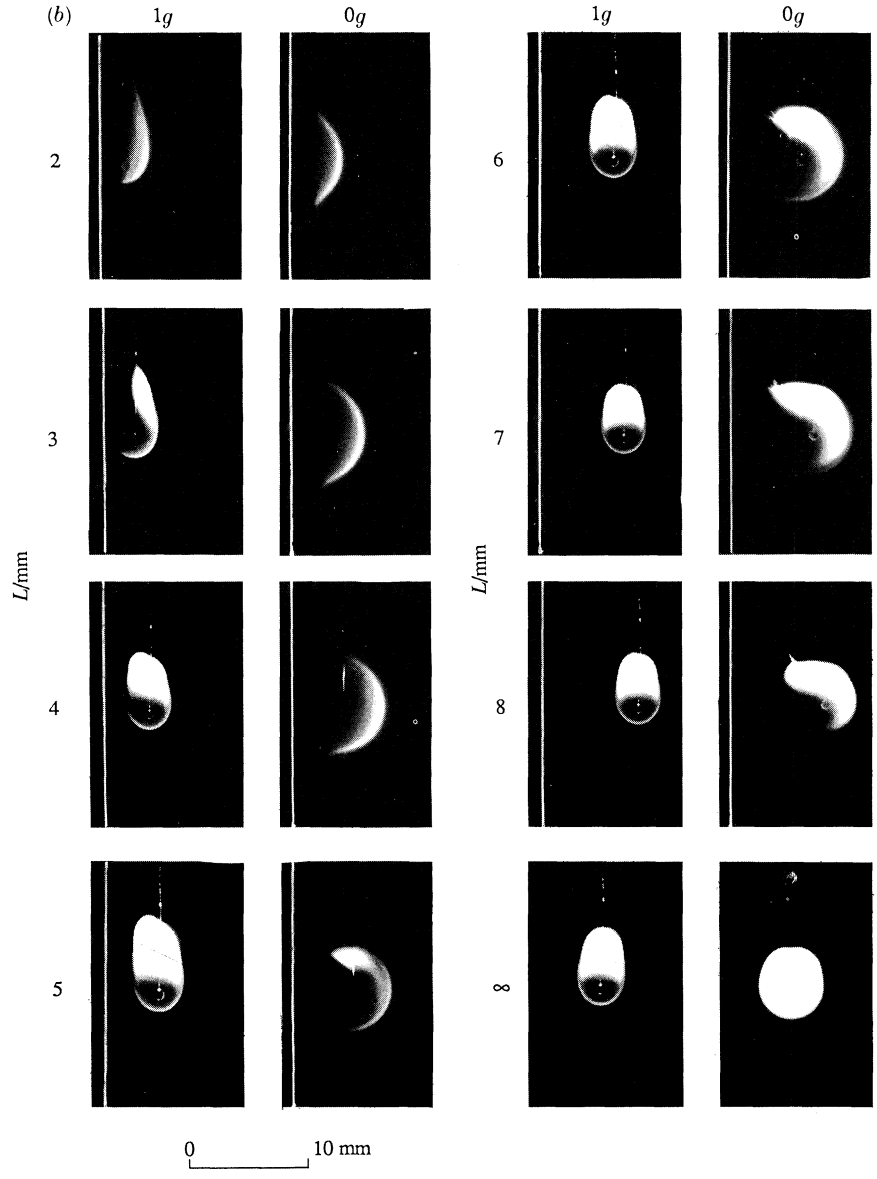

FIGURE 6. (*a*) The flame shape, 330 ms after ignition, around a burning droplet suspended over a horizontal surface at both normal gravity (1*g*) and low gravity (0*g*). (*b*) The flame shape, 330 ms after ignition, around a burning droplet suspended near a vertical surface at both normal gravity (1*g*) and low gravity (0*g*).

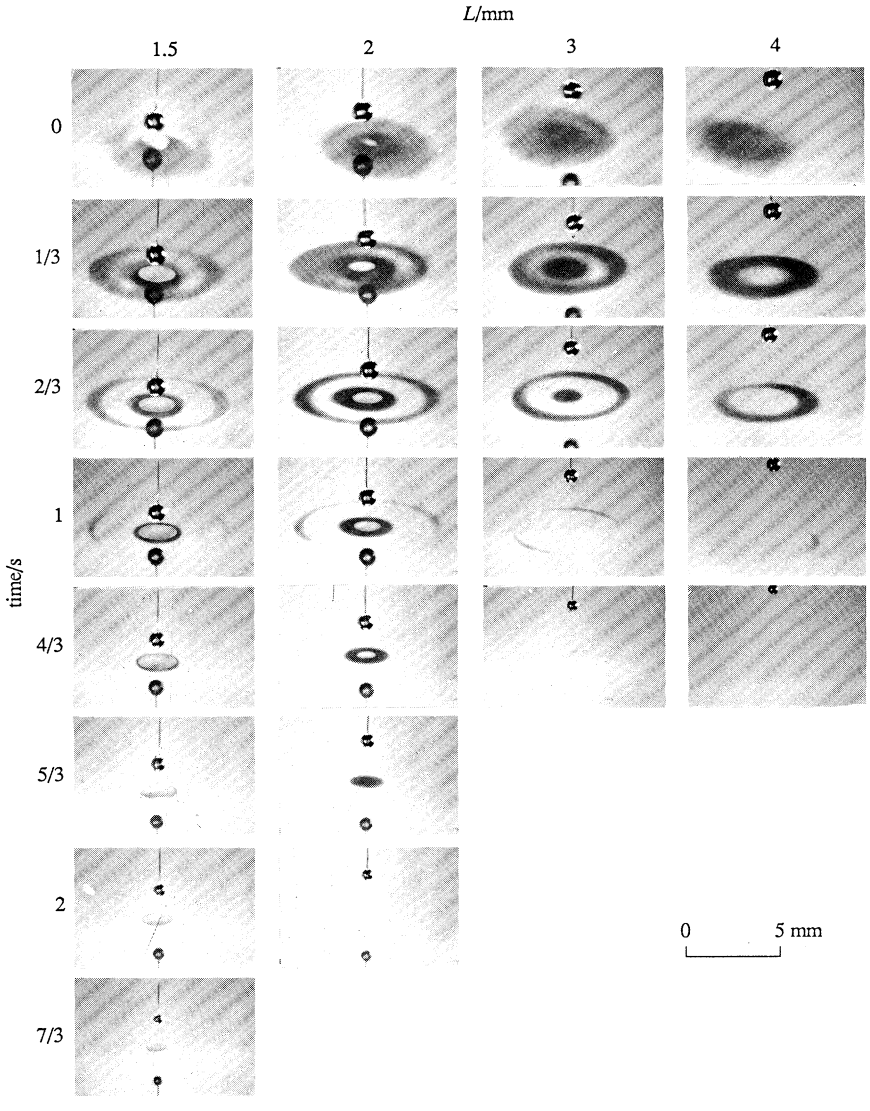

FIGURE 12. Vapour condensation on a horizontal surface below a burning droplet.

(*Facing p.* 491)

increasing luminosity and amount of soot formed around the droplet as the droplet resides farther out from the solid surface. At $L = \infty$ soot radiation completely obscures the flame for the film used, though it has been suggested that for droplets far from solid surfaces the flame may reside inside the sooting zone (Randolph & Law 1986).

Soot particles were observed to be carried through the flame (e.g. figure 6*a* at $L = 7$ mm and 8 mm), predominantly in the wake, by the Stefan and the buoyancy induced flow of vapour around the droplet (in the absence of buoyancy, the motion of soot particles would be radial). The soot particles may act as a heat sink and thereby reduce heat transfer to the droplet. The amount of fuel vapours surrounding the droplet may then be reduced accordingly, the flame might then reside closer to the droplet surface and $(L/D)_{\mathrm{crit}}$ would then be lower than in the absence of any soot formation.

The flame/soot shapes shown in the second column in figure 6 at each value of L are similar to the shapes predicted by (2) (cf. figure 4), though quantitative comparisons are not favourable for the same reasons that measured values of $(L/D)_{\mathrm{crit}}$ cannot be predicted as noted above. The flame shapes at low gravity are essentially the same for the 'horizontal' and 'vertical' surfaces as expected, because orientation effects should be absent within a low enough gravity environment.

The sooting zone is nearly spherical when $L = \infty$ (cf. figure 6*a* and *b*) but the flame is not visible at this distance due to the intense luminosity from the soot. Observations (not shown) of a non-sooting fuel (methanol) at $L \to \infty$ confirmed the expectation of a spherical flame boundary in our low gravity environment. Some vertical elongation of the methanol flame, similar to that observed under Earth normal gravity conditions for heptane (cf. figures 5 and 6) was noted near the termination of the experiment (i.e. as time $\to 1.2$ s for an initially 1.1 mm diameter droplet). This elongation is conjectured to be due to an increase in the buoyancy level in the moving frame of reference caused by g/g_{o} increasing from 0 at the instant of release of the package to about 10^{-3} at the instant of impact. This increase is caused by air drag around the falling package.

The burning rate K was inferred from measurements of the evolution of droplet diameter. Such measurements may perhaps be useful provided that the evolution of the square of droplet diameter is linear during burning. Such linearity in reality exists only over a portion of the burning history due to effects of droplet heating which arise immediately after ignition, and extinction which may sometimes occur. Since K is obtained by differentiating the data, its value is extremely dependent on the amount and accuracy of the data used to define it. In our low gravity experiments K was obtained from droplet diameter data (Chandra 1990) which only spanned between 40 to 60% of the total burning history due to termination of the period of observation because of the relatively low experimental time (about 1.2 s) commensurate with the initial volume of liquid suspended on the quartz fibre. However, the near linearity of the evolution of droplet diameter observed in the present experiments may provide a basis for inferring that K may not be substantially different than values obtained from droplet diameter data which spanned a larger fraction of the burning history (unless extinction occurs or

the droplet experiences a varying ambient oxygen field during its combustion lifetime).

The combustion rate measurements are summarized in figure 7. The curves drawn through the data, as in all subsequent figures, are curves of best fit. The results show that (1) the variation of low gravity burning rates with distance of the droplet from the surface agree qualitatively, but not quantitatively, with (4) (dotted line in figure 7), (2) the burning rate was found to be independent of surface orientation when the experiments were performed in a low gravity environment, (3) the droplets burned faster at Earth normal gravity when they were placed near a vertical surface than a horizontal surface, and (4) the asymptotic burning rate, K_∞, was higher for burning at Earth normal gravity than at low gravity.

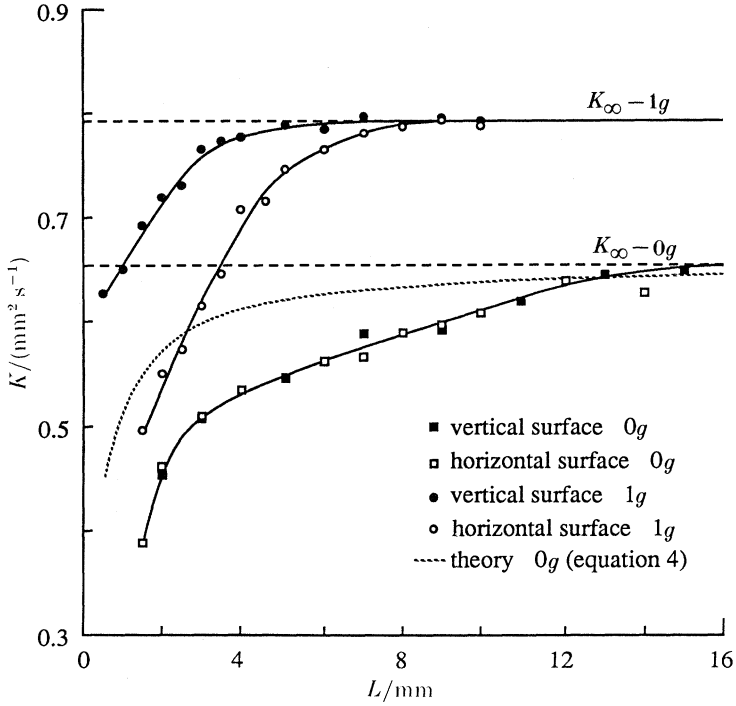

FIGURE 7. Combustion rate variation with L.

In the absence of a bouyancy induced flow around the droplet, the measured burning rate decreased as L decreased and the burning rate for a droplet residing near a vertical surface ($K \to K_\mathrm{v}$) was essentially indistinguishable from that of a droplet positioned near a horizontal surface ($K \to K_\mathrm{h}$). This latter result is expected for low enough buoyancy (i.e. Grashof number).

The variation of K with L qualitatively conforms with the prediction given by (4), namely that K decreases as L increases. The solid surface distorts the flow field from the spherically symmetric field that would exist when $L = \infty$ such that the streamlines bend due to the presence of the wall. The gas pressure in the region

between the droplet and the solid surface accordingly increases compared to the far field value (which, for a Leidenfrost droplet, provides the force necessary to levitate the droplet above the surface (Nguyen & Avedisian 1987)) which makes it more difficult for air to diffuse to the region between the droplet and the solid surface. The resulting lack of a stoichiometric air : fuel ratio in that region prevents the flame from closing around the droplet in the manner depicted in figure 4*c* and in, for example, frame $[3, \frac{1}{3}]$ in figure 5*a* so that the heat supply to the droplet decreases accordingly. The effect is more pronounced and the flame opening is wider as L decreases so that K progressively decreases as L decreases. The variation of λ with ξ^* given by (4) mathematically expresses this fact.

In the presence of a buoyancy induced flow around the droplet, the burning rate was again observed to decrease as L decreased. Now, though, $K_v \neq K_h$ and K_v is greater than K_h; the burning rates for both the horizontal and vertical surface are higher than for burning at low gravity.

The higher droplet combustion rate near a vertical surface than a horizontal surface might at once imply that the vapour velocity over a droplet that is burning near a vertical surface is greater than the buoyancy induced gas velocity flowing past a droplet burning near a horizontal surface. That such may be the case can be argued from the perspective of a line source placed near, in turn, a vertical surface and a horizontal surface: the gas velocity near a line source placed adjacent to a vertical surface increases as L decreases (Pera & Gebhart 1975) whereas the opposite is true for a horizontal surface (Reimann 1974). Although no direct measurements were made of gas velocities around the burning droplets, the height of the flame around a burning droplet has been shown to provide a measure of the vapour flow (Isoda & Kumagai 1959).

Figure 8 shows measured flame heights H_F normalized by the flame height for a droplet burning far from the surface $H_{F,\infty}\,(= H_F(L \to \infty))$. The flame height is defined in the inset to figure 8 and the measurements were made $\frac{1}{3}$ s after ignition for illustration. It is seen that for burning near a horizontal surface the flame height (i.e. the gas velocity around the droplet) decreases as L decreases while the opposite is true for a droplet burning near the vertical surface. The expectation might then be that K_v should increase as L decreases, or perhaps exhibit an extremum as L decreases from infinity due to the competing influence of restricted oxygen supply to the region between the droplet and the solid surface, discussed above, as L decreases. That in fact K_v decreases only (with the magnitude of the decrease not being as large as that of K_h so that as observed $K_v > K_h$) suggests that the dominant influence on the burning rate may be the progressive restriction of the oxidizer flow from the far field to the region between the droplet and the solid surface as L decreases. The additional effect of heat loss, to what is in reality a non-adiabatic solid surface in the present experiments, would serve to further reduce K_v as L decreases.

A factor not explored in the present study is the effect of initial droplet volume (i.e. initial diameter) on the burning rate. At Earth normal gravity the burning rate of suspended droplets of *n*-heptane has been shown to increase as the initial droplet diameter increases (Monaghan *et al.* 1968). Under low buoyancy conditions the initial droplet size may still influence the burning rate by its effect on the heat

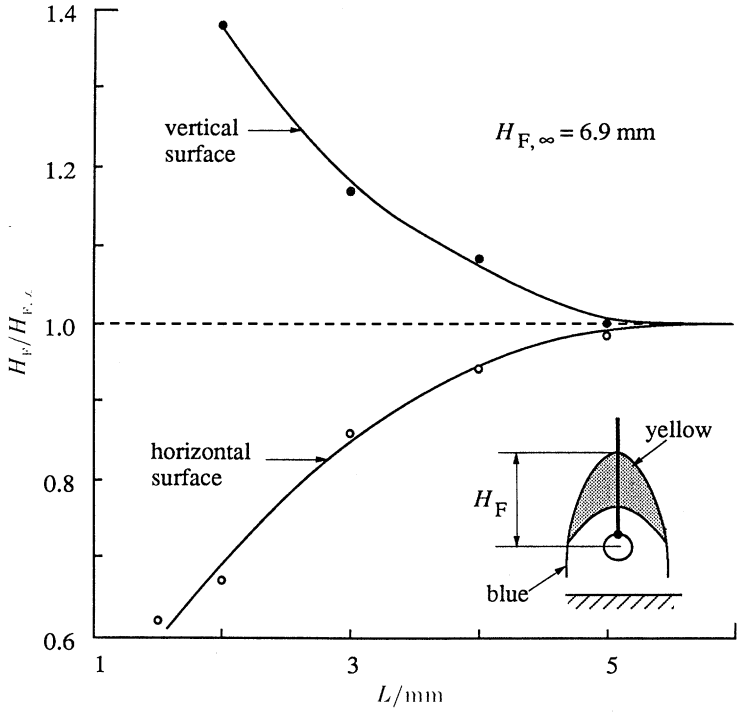

FIGURE 8. Normalized flame height variation with L.

transfer to the droplet through the presence of soot in region between the droplet and flame. As the initial droplet diameter decreases the flame may regress towards the droplet surface faster than the soot, thus overtaking the soot and oxidizing it. A soot shell may therefore not exist around a small droplet (Randolph & Law 1986); the opposite could be true for a large droplet. The formation of soot by pyrolysis is an endothermic process and a soot shell may also provide a thermal barrier to heat transfer from the flame to the droplet. We could therefore envision the droplet burning rate decreasing as the initial droplet diameter increases because of the presence of a soot shell, though no support for this conjecture was obtained in the present study because the initial equivalent diameter of the droplet was held constant.

3.2. *Effects of heat losses to the solid surface*

That the surface is non-adiabatic can be demonstrated by noting that for heat transfer into a horizontal quartz surface from a hot ambient gas at the adiabatic flame temperature, the order of magnitude of the Biot number is 0.7; it is somewhat less for a vertical surface (Incropera & De Witt 1981). Heat is transferred into the solid surface so that the measured burning rate should be less than it would be for an adiabatic surface. However, the heat loss reduces not only the burning rate but also the flame temperature and could consequently affect the rate of soot formation and fuel combustion. The overall impact of heat transfer to the solid surface on the droplet combustion may therefore be complex.

Regardless of the mechanisms of heat transfer from the flame to the solid surface (conduction, convection, or radiation) the magnitude of the heat transfer is controlled by the temperature difference between the hot combustion gases, T_f, and the relatively cold surface, T_s. An appropriate measure of heat transfer to the surface is given by the simplest constitutive equation between heat flux and temperature difference, namely that of one-dimensional conduction. The model is based on the flame and the surface being considered as two infinite parallel planes which are separated by a vapour layer of thickness ϵ.

Maximum gas temperatures surrounding a droplet burning at normal gravity were measured using a platinum–10 % rhodium thermocouple. The thermocouple bead was positioned along a line passing through the centre of the droplet, parallel to the surface (inset to figure 9). The droplet was ignited and the gas temperature was recorded using a digital oscilloscope as the flame swept past the thermocouple bead. This procedure was repeated with the thermocouple relocated at 0.2 mm intervals along the line $\theta = 0°$ for a drop near a vertical surface, and the line $\theta = 90°$ for a drop above a horizontal surface, where θ is the angle measured from the bottom of the drop. The maximum gas temperature, measured along each traverse of the thermocouple, was identified with a characteristic flame temperature.

As the surface was brought closer to the drop ($L < \infty$), T_f was reduced for both a horizontal and vertical surface as expected because of heat losses to the surface. For a droplet with no surface present ($L = \infty$), the gas temperature at $\theta = 90°$ is

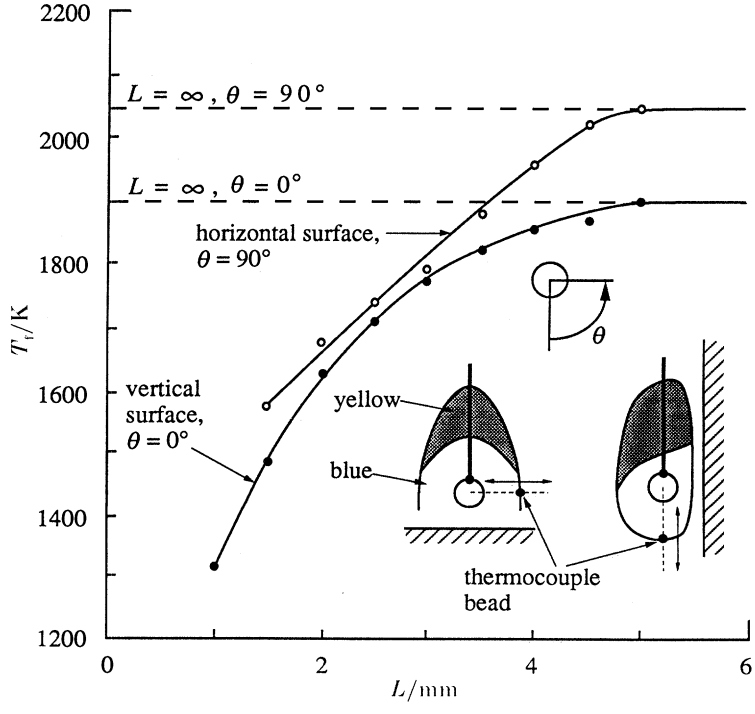

FIGURE 9. Characteristic flame temperature variation with L.

higher than at $\theta = 0°$, as shown in figure 9, possibly because of increased heating by combustion gases rising from below. The magnitude of the temperature reduction was approximately the same for the two surface orientations studied. This reduction in flame temperature as L decreases may also explain the change in flame colour observed as L decreases in figure 5.

As the droplet was brought closer to the surface, the flame colour became progressively more blue as shown in figure 5, thus revealing a reduction in soot formation. This fact is in agreement with previous investigations that have shown the rate of soot formation in diffusion flames to be strongly dependent on temperature (Glassman & Yaccarino 1981), such that as flame temperature decreases the amount of soot formed is reduced. The distance from the centre of the drop to the start of the yellow luminous zone, H_L as defined in figure 10, provides a qualitative measure of the tendency of the flame to soot. H_L was measured along the flame centreline $\frac{1}{3}$ s after ignition for various L. The variation of H_L/H_F with T_f is displayed in figure 10. It has been suggested, based on experimental observations, that soot formation takes place along the centreline of a diffusion flame when the centreline temperature is above a critical value of 1350 K (Gomez *et al.* 1987). The present results appear to offer some support for this conclusion. As the flame temperature decreases below the critical temperature, $H_L/H_F \to 1$, that is, the flame becomes entirely blue which indicates an absence of soot radiation.

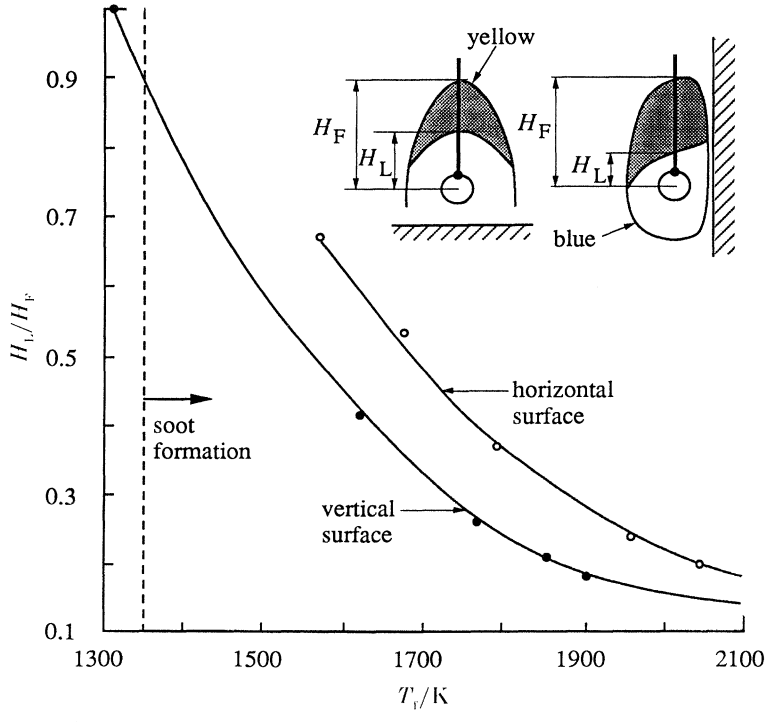

FIGURE 10. Change in soot formation, as measured by the fraction of the flame height along the centreline that is blue, with flame temperature.

The surface temperatures T_s were measured using a platinum thin film sensor at only one point on the surface which was directly in line with the droplet centre. Figure 11 displays the evolution of surface temperature during droplet combustion at normal gravity at the indicated value of L. The change in surface temperature $\Delta T_s\,(=T_s(t)-T_s(0))$ is shown as a function of time where $T_s(0)=20\pm2$ °C. The droplet was ignited at $t=0$ s. The surface temperature continues to increase as long as there is a net positive heat input into the surface; i.e. as long as the heat input from the flame to the surface exceeds the losses from the surface to the ambient. For small L, the conduction distance from the flame to the surface is small, so that the heat input would be expected to dominate losses throughout the burning history. The surface temperature would therefore continue to rise until burning is complete, and the peak temperature would coincide with the end of burning. As L increases the heat input from the flame is reduced, and losses may exceed the heat input before the end of combustion. Support for this hypotheses is offered by the surface temperature traces (figure 11*a* and *b*), which show that for $L\leqslant 2$ mm the time at which the peak temperature is reached coincides with the end of the droplet burning as measured from observations by using a video system (indicated by a dotted vertical line in figure 11). As L increases, losses exceed heat input earlier in the burning history, and therefore the temperature peak precedes the end of droplet combustion. There was no measurable increase in surface temperature for $L>7$ mm, corresponding to the distance at which the droplet burning rate became the same as that of a droplet in a unbounded ambience ($L\to\infty$ in figure 7).

In view of the fact that $T_f\gg T_s$ as shown in figures 9 and 11, and further assuming that $\epsilon\approx L$, the heat flux between the flame and the solid surface, q_s, can be expressed as

$$q_s\sim k_v\,T_f(L)/L. \tag{5}$$

The inverse relation between q_s and L explicit in the constitutive relation of (5) for a conduction mechanism (but still also implicit for convection and radiation) reveals the interesting prospect that q_s may exhibit an extremum as L decreases from infinity. For $L>5$ mm, T_f is constant (figure 9) and q_s should therefore increase as L decreases. However, for $L<5$ mm T_f decreases (figure 9) and if the rate of this decrease is faster than that of L, q_s will decrease as well, hence the extremum. That such an extremum in q_s may exist was noted from an alternative perspective of assuming the surface to be a semi-infinite body in which heat transfer to the surface was by one dimensional heat conduction normal to the wall. In this case, q_s could be calculated by knowing only the evolution of $T_s(t)$ (Hall & Hertzberg 1958), data for which are shown in figure 11 at one location on the quartz surface.

The fact that the heat loss may first increase and then decrease as the droplet is brought progressively closer to the wall may lead one to expect a change in the slope of the variation of K with L. This possibility could not be discerned from our burning rate data because its identification would require accurately measuring the second derivative of the variation of D^2 with time.

The spectrum of flame configurations – opened or closed – that may exist around the droplet during burning, and the relatively low values of T_s, suggest

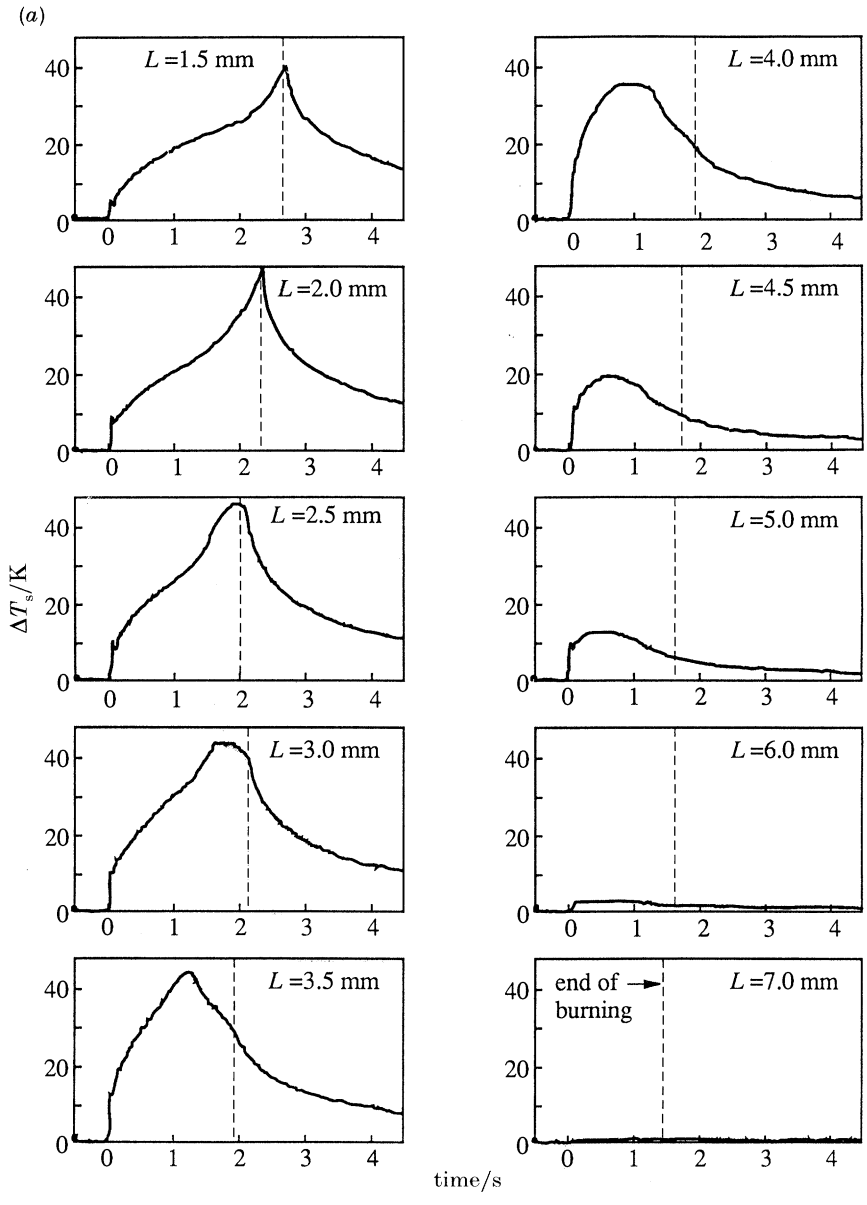

FIGURE 11*a*. For description see opposite.

that fuel could condense on the solid surface during burning. Figure 12, plate 5, shows a series of 35 mm photographs of such condensation over a horizontal surface at normal gravity; similar observations (not shown) were recorded for a droplet adjacent to a vertical surface. Due to the bright lighting used, the flame surrounding the droplet is not visible, though the photographs correspond to the sequences in figure 5*a* in which the flame can be seen. The photographs in each

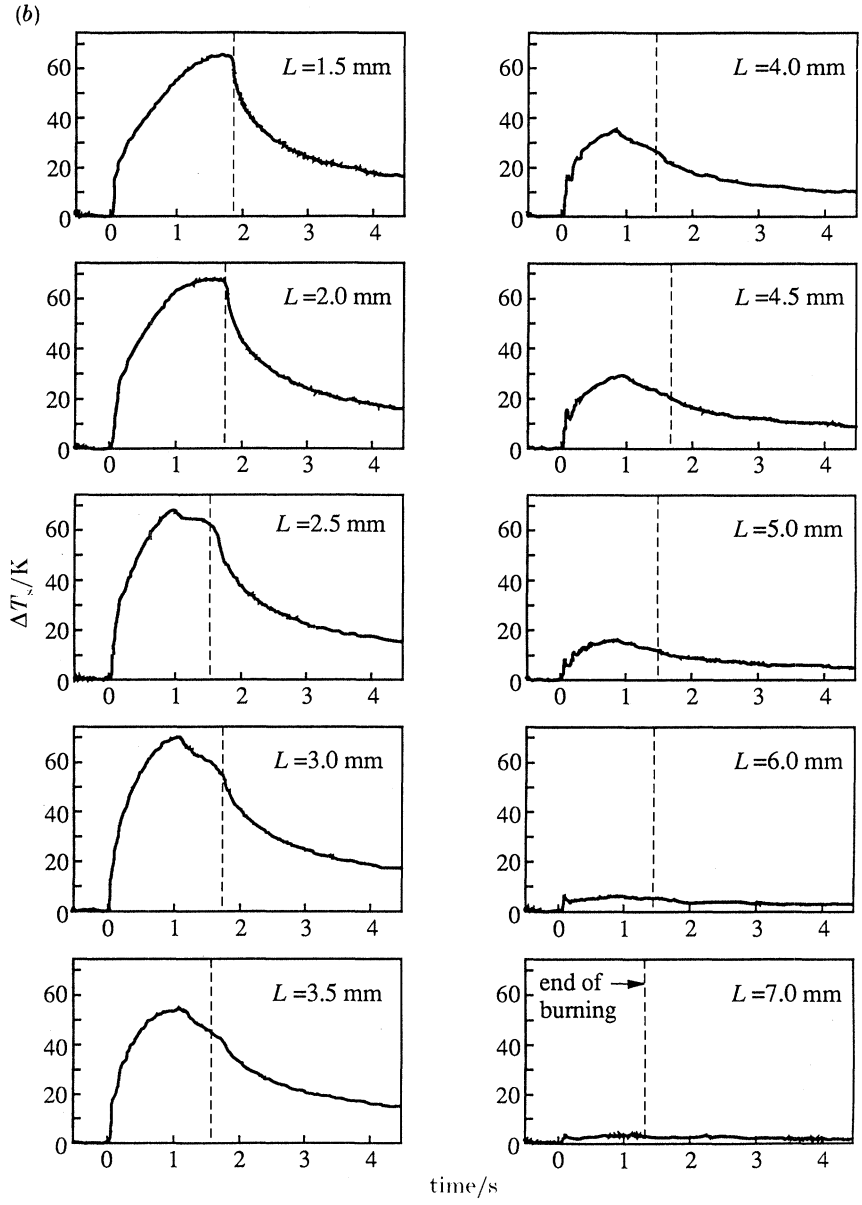

FIGURE 11. (*a*) Oscilloscope traces showing surface temperature variation of a horizontal surface below a burning droplet. (*b*) Oscilloscope traces showing surface temperature variation of a vertical surface near a burning droplet.

sequence were taken at a rate of 3 frames per second. The first frame in each series shows droplet ignition.

Condensation of fuel was believed to be revealed by a shining lens-like patch of liquid immediately below the drop. Surrounding the fuel were two concentric dark rings which were assumed to be water condensate. To confirm this conjecture, the surface temperature was raised to 110 °C and a hexadecane droplet (boiling point

of 288 °C) was ignited. A central patch of liquid was still observed to condense during droplet combustion even though the surface temperature was high enough to evaporate any water condensate. No dark rings were seen in this case.

At $L = 1.5$ mm the water condensate appeared to evaporate first, leaving behind a diminishing pool of fuel beneath the drop. When L was increased to 2 mm, the fuel condensate evaporated first leaving behind water underneath the drop. For $L \geqslant 3$ mm, no fuel condensation was observed during the entire combustion period.

A simple criterion for fuel vapours to condense at a solid surface adjacent to which a droplet is burning can be based on comparing the time of flight of a fuel 'packet' from the droplet surface to the solid surface, t_r, with the characteristic time t_c for the packet to be consumed by chemical reaction during its transit to the surface. Defining a Damköhler number as

$$Da = t_r/t_c \tag{6}$$

if $Da \gg 1$, the fuel reacts before it reaches the surface so no condensation occurs. If $Da \ll 1$, the fuel could reach the surface before it reacts.

If the fuel vapours moving at velocity v_s travel a distance δ from the droplet to the solid surface, t_r is approximated as

$$t_r = \delta/v_s, \tag{7}$$

where δ is the minimum distance between the droplet and the surface. For a horizontal surface $\delta = L - D_0$ and for a vertical surface $\delta = L - \frac{1}{2}D_0$. v_s is a characteristic velocity with which fuel vapour leaves the droplet surface, measured at the start of combustion. For example, $v_s \sim \mathring{m}/\rho_v$.

A characteristic time for combustion of fuel vapour is defined by

$$t_c = [F]/[\mathring{F}]. \tag{8}$$

As an approximation, $[F]$ is taken to be the average fuel concentration around the droplet corresponding to a mole fraction of 40 % (Law & Williams 1972), with the remainder of the gas being air. $[\mathring{F}]$ is the fuel consumption rate and is approximated by a single-step reaction rate for the combustion of n-heptane of the form (Westbrook & Dryer 1981)

$$[\mathring{F}] = 5.1 \times 10^{11} \exp(-30/RT)\,[F]^{0.25}[O_2]^{1.5}, \tag{9}$$

where the units are centimetre second mole kilocalorie kelvins. The reaction rate was evaluated at the maximum gas temperature which was measured between the droplet and the surface.

The calculated variation of Da with δ is shown in figure 13, and agrees qualitatively with the experimental observation that fuel vapour condensed on the surface for $\delta \leqslant 0.9$ mm when $Da \approx 10^{-2}$ whereas no condensation was seen for $\delta \geqslant 1.45$ mm ($Da \approx 10$).

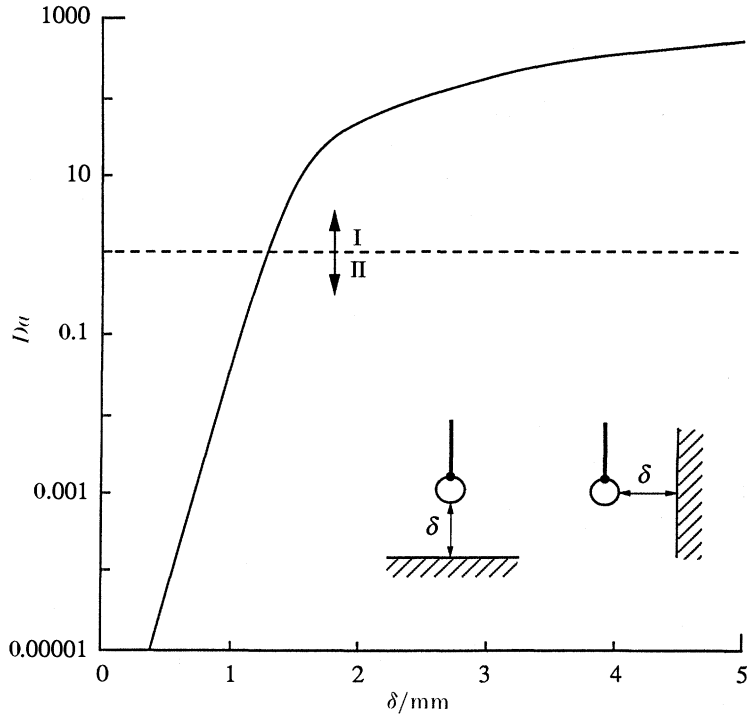

FIGURE 13. Variation in Da with δ. Region I, no fuel vapour condensation; region II, fuel vapour condensation on surface.

3.3. *Implications for a droplet moving towards a surface*

The present experimental results were obtained for a droplet held at a fixed distance from a cold surface. In practical applications the distance of the droplet from the surface may be changing with time such as in spray combustion wherein the droplets are burning while moving about within the combustion chamber.

When a burning droplet moves towards a surface, both the flame configuration and burning rate will change as the droplet gets progressively closer to the surface. For example, in the dilute droplet region of a spray within which a flame envelop would exist around the droplet, the flame will initially be closed around the droplet surface (figure 4*c*) but then open (figure 4*a*) for some instant before impact of the droplet with the surface. If the droplets are moving very slowly and quasi-steady burning conditions prevail, the results of the present study can provide insights into expectations for moving droplets under those conditions. Consider, for example, the burning rate.

The variation of K with L was isolated in the present study by holding other system parameters constant (ambient and initial solid surface temperature, initial droplet volume, and fuel composition). From the Earth normal gravity data in figure 7, K can be expressed in the form

$$K = K_\infty(1 - C_1 \exp(-C_2 L)), \tag{10}$$

where C_1 and C_2 are constants. Least squares approximations of the data shown in figure 7 yield $C_1 = 0.99$ and $C_2 = 0.55$ for a horizontal surface and $C_1 = 0.22$ and $C_2 = 0.52$ for a vertical surface.

Now if a droplet is moving with a constant velocity v_a toward the solid surface, then K will change instantaneously (in the quasi-steady limit) commensurate with a change in L and exhibit a time dependence through the variation of L with t since $L \sim v_a t$. As an example, a droplet which is initially 1.1 mm in diameter that is approaching a horizontal surface from a position 10 mm above the surface is considered. With $K = -\mathrm{d}D^2/\mathrm{d}t$ and $L = L_0 - v_a t$, (10) was solved numerically. Figure 14 shows the calculated evolution of diameter corresponding to approach

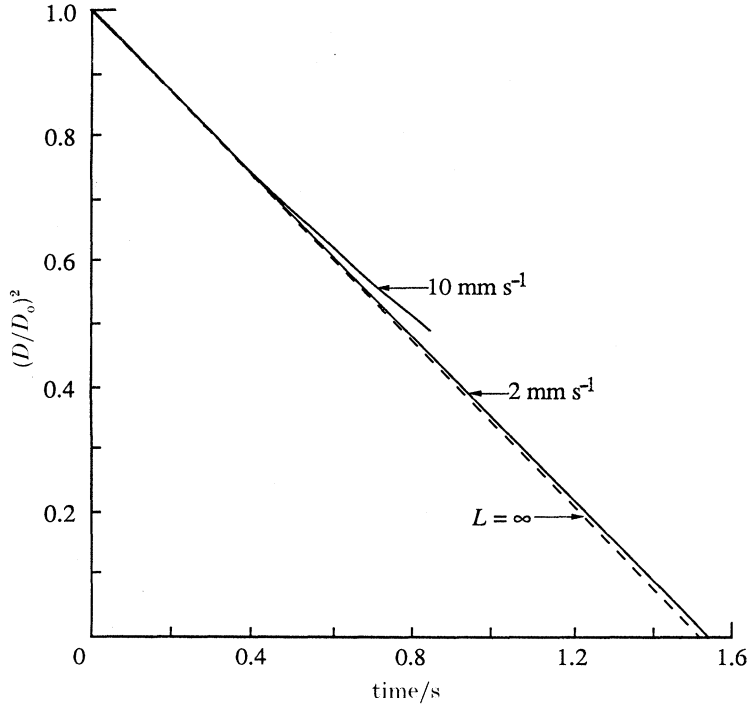

FIGURE 14. Evolution of normalized droplet diameter squared for a droplet approaching a horizontal surface.

velocities of 2 mm s^{-1} and 10 mm s^{-1}. At the smaller velocity the droplet moves about 3 mm during its burning history and the evolution of droplet diameter is nearly the same as for $L = \infty$ (dotted line). At 10 mm s^{-1}, the droplet moves through a wider region of influence of L on K so that K changes more substantially and the evolution of D^2 is more perceptibly nonlinear. However, in this case the period of free burning is terminated before burnout because the droplet impacts the surface.

We thank Mr Gregory Jackson for his help with some of the experiments. Additional conversations with Dr James E. Anderson of Ford have been helpful.

This work was supported by the National Science Foundation through grant no. CBT-8451075 and the New York State Center for Hazardous Waste Management. This support is gratefully acknowledged.

References

Avedisian, C. T., Yang, J. C. & Wang, C. H. 1988 *Proc. R. Soc. Lond.* A **420**, 183–200.
Chandra, S. 1990 Ph.D. thesis, Cornell University, U.S.A.
Chandra, S. & Avedisian, C. T. 1988 *Proc. R. Soc. Lond.* A **418**, 365–382.
Glassman, I. & Yaccarino, P. 1981 *18th Symp. Int. Combustion*, pp. 1175–1183. Pittsburgh, Pennsylvania: The Combustion Institute.
Gomez, A., Littman, M. G. & Glassman, I. 1987 *Comb. Flame* **70**, 225–241.
Gottfried, B. S., Lee, C. J. & Bell, K. J. 1966 *Int. J. Heat Mass Transfer* **9**, 1167–1187.
Hall, J. G. & Hertzberg, A. 1958 *Jet Propulsion* **28**, 719–723.
Isoda, H. & Kumagai, S. 1959 *7th Symp. Int. Combustion*, 523–531. London: Butterworths.
Incropera, F. P. & De Witt, D. P. 1981 *Fundamentals of heat transfer*, pp. 442–446. New York: Wiley.
Karasawa, T., Shiga, S. & Kurayabashi, T. 1986 *Bull. JSME* **29**, 143–148.
Kaskan, W. E. 1957 *6th Symp. Int. Combustion*, pp. 134–143. New York: Reinhold.
Kent, J. H. 1970 *Comb. Flame* **12**, 279–282.
Kumagai, S., Sakai, T. & Okajima, S. 1971 *13th Symp. Int. Combustion*, pp. 779–785. Pittsburgh, Pennsylvania: The Combustion Institute.
Law, C. K. & Williams, F. A. 1972 *Comb. Flame* **22**, 393–405.
Monaghan, M. T., Siddall, R. G. & Thring, M. W. 1968 *Comb. Flame* **12**, 45–53.
Nguyen, T. K. & Avedisian, C. T. 1987 *Int. J. Heat Mass Transfer* **30**, 1479–1509.
Pera, L. & Gebhart, B. 1975 *J. Fluid Mech.* **68**, 259–271.
Randolph, A. L. & Law, C. K. 1986 *Comb. Flame* **64**, 267–284.
Reimann, J. 1974 *Int. J. Heat Mass Transfer* **17**, 1051–1061.
Tamura, Z. & Tanasawa, Y. 1959 *7th Symp. Int. Combustion*, pp. 509–522. London: Butterworths.
Umemura, A., Ogawa, S. & Oshima, N. 1981 *Comb. Flame* **41**, 45–55.
Vargaftik, N. B. 1975 *Handbook of physical properties of liquids and gases*, pp. 266–269. Washington: Hemisphere.
Westbrook, C. K. & Dryer, F. L. 1981 *Comb. Sci. Tech.* **27**, 31–43.
Williams, F. A. 1985 *Combustion theory*, pp. 62–63. Menlo Park, California: Benjamin–Cummings.

Colour plates printed by George Over Limited, Rugby, U.K.

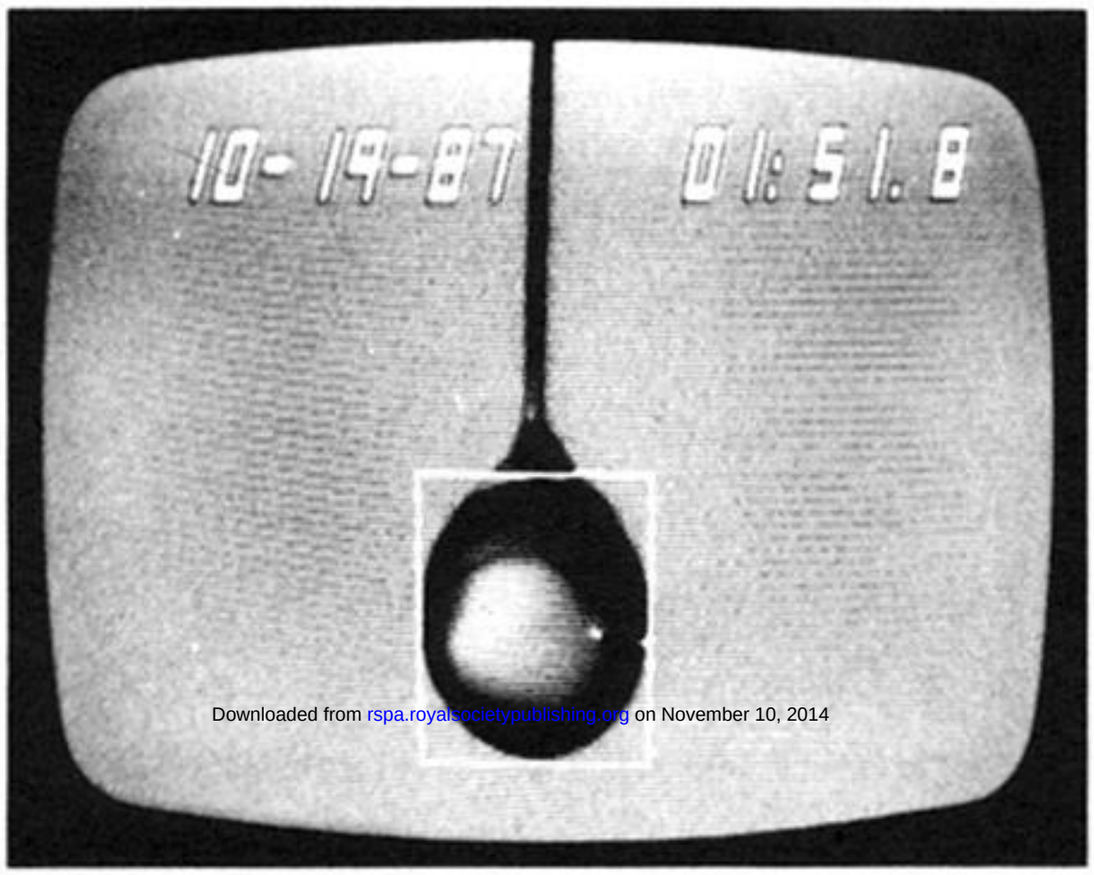

FIGURE 2. (*a*) Video image of suspended droplet under normal gravity at the start of burning. The white rectangle is the video caliper box. (*b*) Definition of lateral and longitudinal diameters at the start of burning. (*c*) Video image showing droplet drawn up the fibre towards the end of burning. (*d*) Diameter definition towards the end of burning.

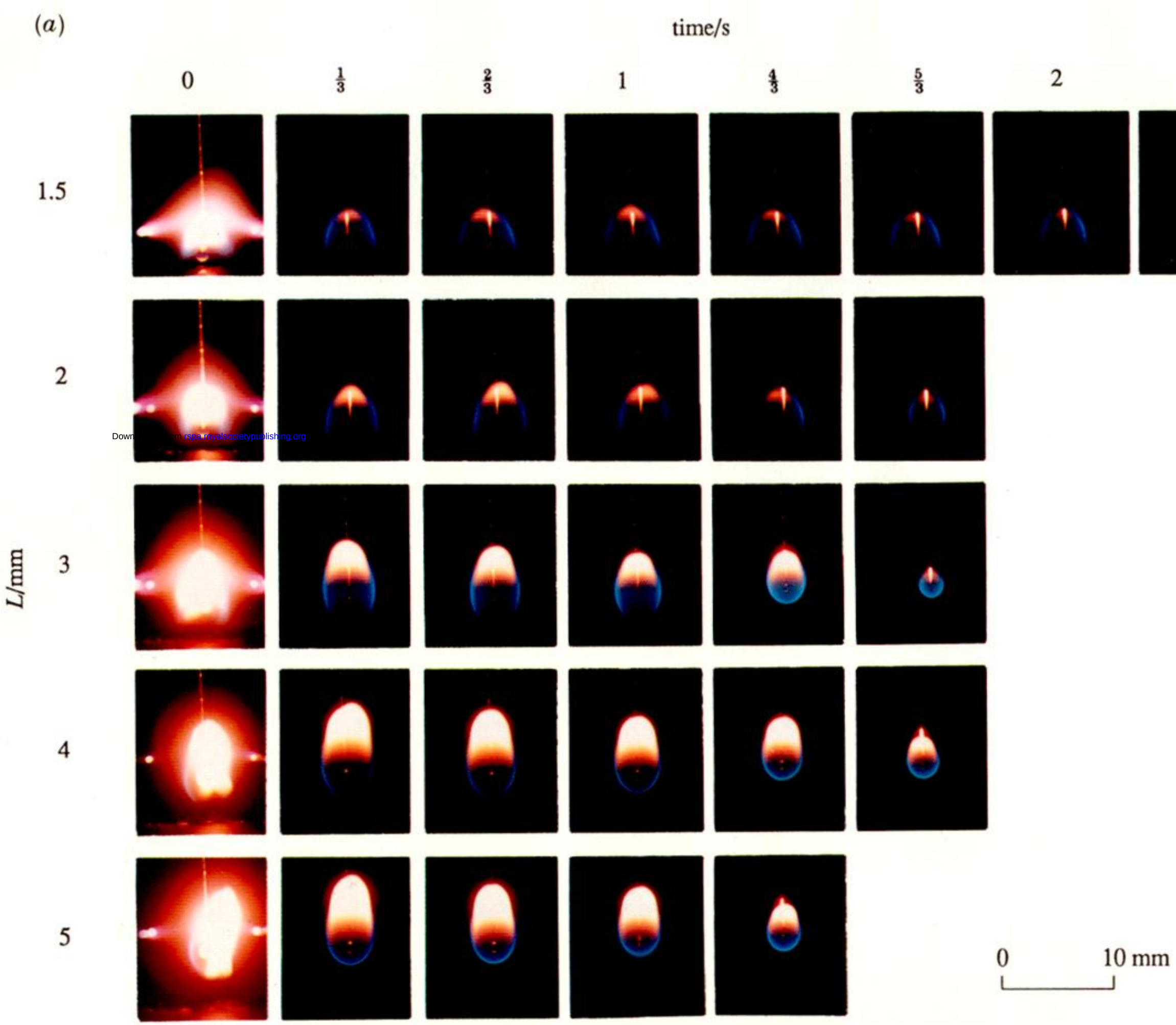

FIGURE 5*a*. Combustion of a droplet suspended over a horizontal surface at normal gravity.

(*b*)

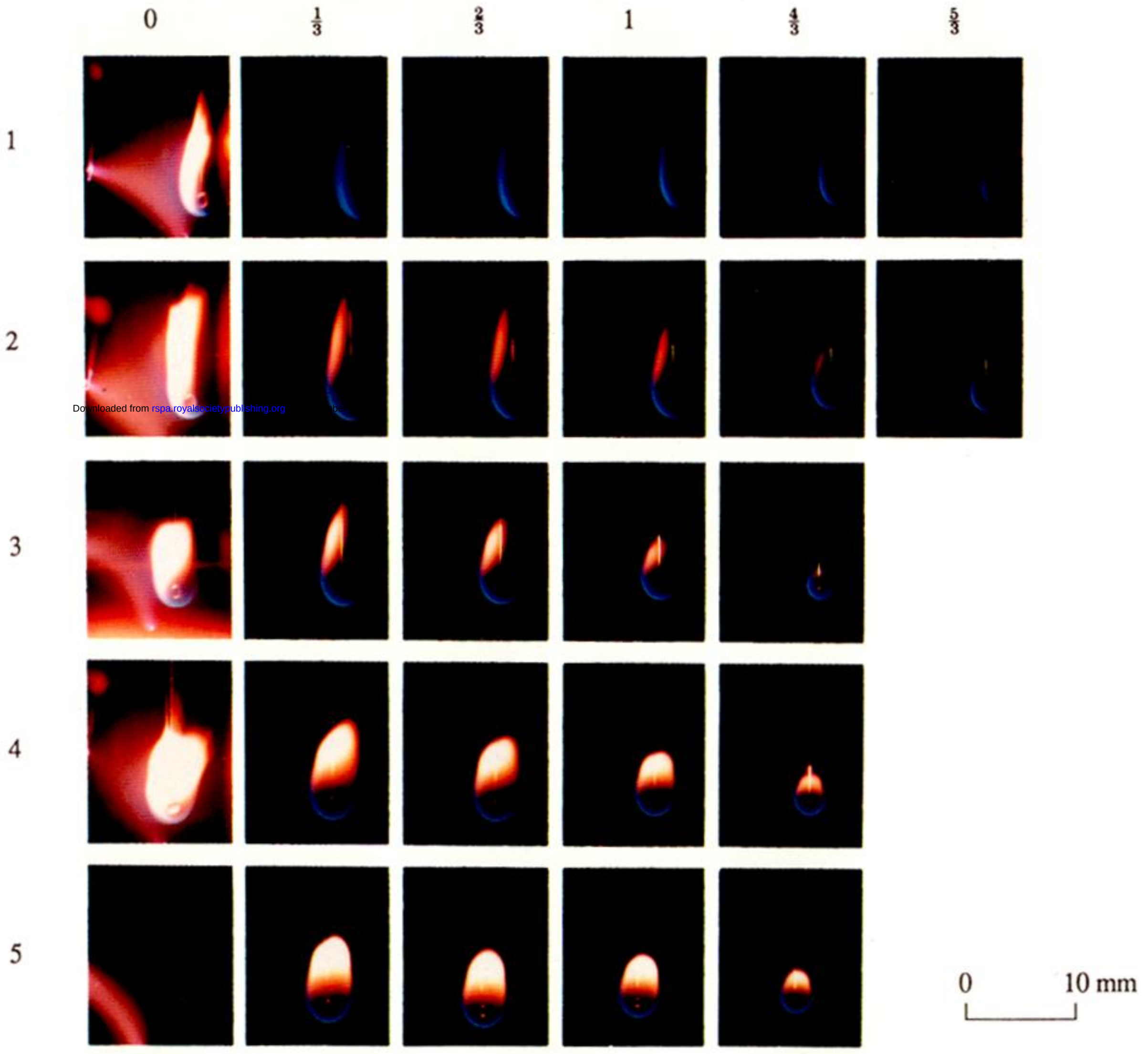

FIGURE 5*b*. Combustion of a droplet suspended near a vertical surface at normal gravity.

Downloaded from rspa.royalsocietypublishing.org on November 10, 2014

FIGURE 6(*a*). For description see opposite.

FIGURE 6. (*a*) The flame shape, 330 ms after ignition, around a burning droplet suspended over a horizontal surface at both normal gravity (1*g*) and low gravity (0*g*). (*b*) The flame shape, 330 ms after ignition, around a burning droplet suspended near a vertical surface at both normal gravity (1*g*) and low gravity (0*g*).

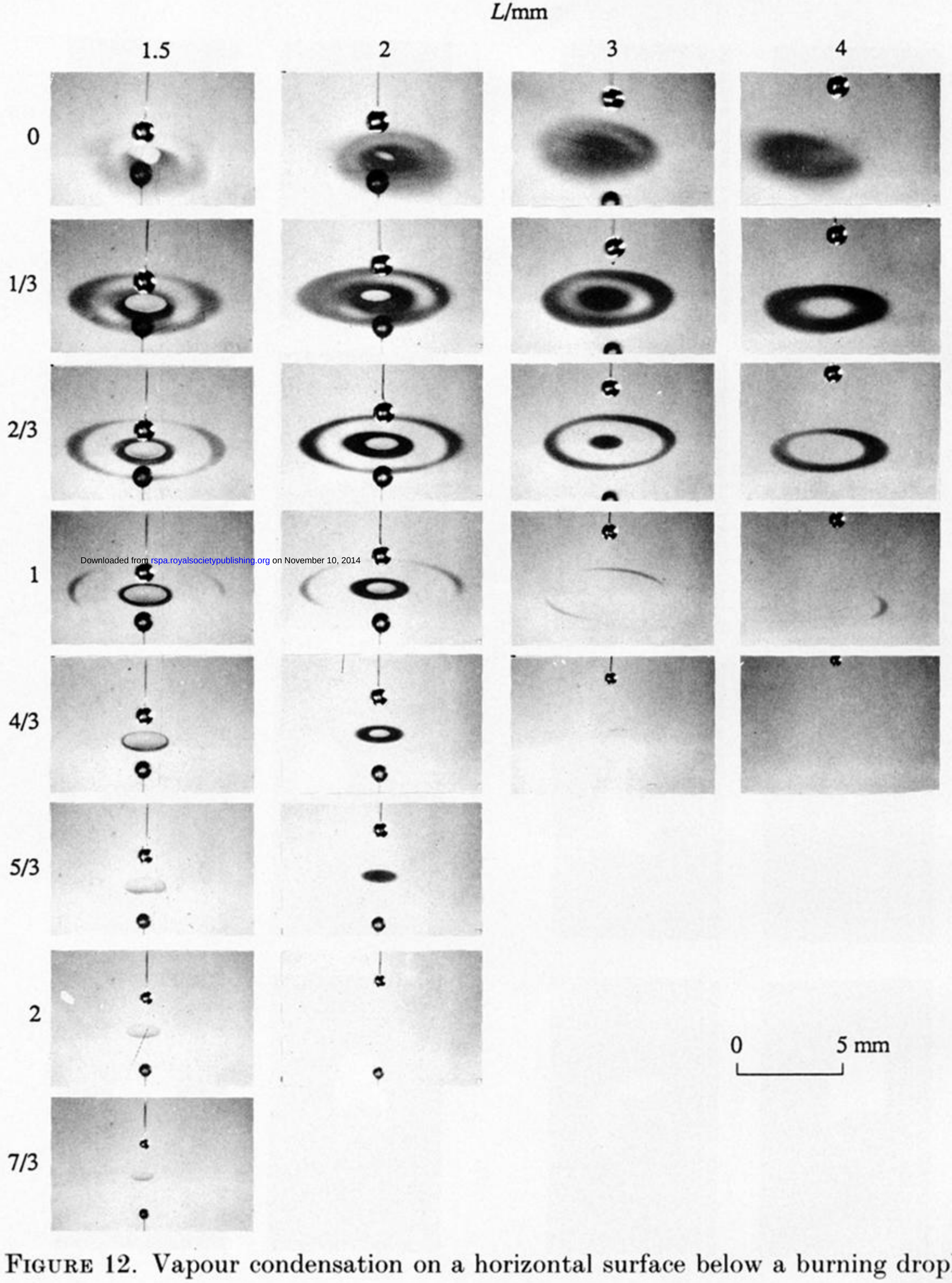

FIGURE 12. Vapour condensation on a horizontal surface below a burning droplet.